High-resolution x-ray structure of human aquaporin 5

Rob Horsefield*†, Kristina Nordén†‡, Maria Fellert‡, Anna Backmark§, Susanna Törnroth-Horsefield*, Anke C. Terwisscha van Scheltinga¶, Jan Kvassman‖, Per Kjellbom‡, Urban Johanson‡, and Richard Neutze*,****

*Department of Chemistry, Biochemistry and Biophysics, University of Gothenburg, Box 462, SE-405 30 Göteborg, Sweden; ‡Center for Molecular Protein Science, Department of Biochemistry, Lund University, Box 124, SE-221 00 Lund, Sweden; §Department of Chemistry and Bioscience, Chalmers University of Technology, Box 462, SE-405 30 Göteborg, Sweden; ¶Department of Structural Biology, Max Planck Institute of Biophysics, 60438 Frankfurt am Main, Germany; and ‖Department of Chemistry and Biomedical Sciences, University of Kalmar, SE-391 82 Kalmar, Sweden

Edited by Douglas C. Rees, California Institute of Technology, Pasadena, CA, and approved June 23, 2008 (received for review February 19, 2008)

Human aquaporin 5 (HsAQP5) facilitates the transport of water across plasma membranes and has been identified within cells of the stomach, duodenum, pancreas, airways, lungs, salivary glands, sweat glands, eyes, lacrimal glands, and the inner ear. AQP5, like AQP2, is subject to posttranslational regulation by phosphorylation, at which point it is trafficked between intracellular storage compartments and the plasma membrane. Details concerning the molecular mechanism of membrane trafficking are unknown. Here we report the x-ray structure of HsAQP5 to 2.0-Å resolution and highlight structural similarities and differences relative to other eukaryotic aquaporins. A lipid occludes the putative central pore, preventing the passage of gas or ions through the center of the tetramer. Multiple consensus phosphorylation sites are observed in the structure and their potential regulatory role is discussed. We postulate that a change in the conformation of the C terminus may arise from the phosphorylation of AQP5 and thereby signal trafficking.

membrane protein | trafficking | crystallography | water channel protein | heterologous overexpression

Aquaporins (1) facilitate the flow of water across cellular membranes while preserving ion concentration gradients. By maintaining water homeostasis within cells, aquaporin family members play essential physiological roles within all kingdoms of life. They form a large superfamily containing both pure water channels, and channels also permeable to other small polar molecules such as glycerol (2). Thirteen human aquaporin (AQP) isoforms have been identified, and they govern a broad spectrum of physiological functions (2, 3). Examples include concentration of urine in the kidneys, release of tears and maintenance of lens transparency in the eye, maintenance of water homeostasis within the brain, the extrusion of sweat from the skin, control of glycerol concentration in fat metabolism, and facilitation of cell migration during angiogenesis.

X-ray and electron diffraction studies have yielded crystal structures of mammalian AQP0 (4–6), AQP1 (7, 8), AQP2 (9), and AQP4 (10), plant SoPIP2;1 (11, 12), bacterial AQPZ (13, 14), and GlpF (15), and the archaeal AQPM (16). These structures establish that phylogenetically and functionally diverse AQPs arrange as homotetramers, each protomer containing six highly conserved transmembrane (TM) α-helices. Two half-helices form a pseudoseventh TM helix because of the insertion of loops B and E into the membrane from opposite sides, placing both copies of the highly conserved Asn-Pro-Ala (NPA) AQP signature motif near the center of the water channel. The conserved aromatic/arginine (ar/R) constriction region imposes substrate selectivity on the channel (17). A consensus has emerged from molecular dynamics simulations regarding the mechanism of water transport and ion exclusion (18) establishing that an electrostatic potential barrier peaking at the NPA region prevents the cotranslocation of protons through the channel.

Although the tissue-specific expression of human AQPs is tightly regulated at the transcription level, certain isoforms are also regulated by posttranslational modifications (19). For example, phosphorylation events appear to trigger the membrane specific trafficking of AQP1 (20), AQP2 (21), AQP5 (22–24), and AQP8 (25), and the gating of AQP4 (26). Nevertheless, structural details concerning the molecular mechanisms of human AQP regulation are unknown.

To better understand distinguishing features of the human AQPs, we crystallized and solved the x-ray structure of human AQP5 to 2.0-Å resolution. This water-specific AQP has been identified within cellular membranes of the stomach, duodenum, pancreas, airways, lung, salivary glands, sweat glands, eye, lacrimal glands, and inner ear (2, 3, 27). As with HsAQP2, its closest paralog, sharing 63% amino acid sequence identity, HsAQP5 has been implicated in trafficking from intracellular membranes to the apical membrane of epithelial cells after C-terminal modifications (24, 28) and in response to the addition of cAMP (22, 24) or cevimeline (23). Sjögren syndrome, for which patients suffer from dry eyes and mouth, represents a clinical manifestation of defective HsAQP5 trafficking (29). Several amino acid residues important for gating the plant AQP SoPIP2;1 are also conserved in AQP5 (19), although functional evidence in support of AQP5 gating is lacking. Our structure reveals the conformation of four consensus phosphorylation sites and highlights structural themes that recur across eukaryotic AQPs. An ordered lipid molecule is also observed within the putative central pore. The significance of these findings regarding the functional role of the central pore and the regulation of human AQPs is discussed.

Results

Crystallization of AQP5. HsAQP5 was cloned into *Pichia pastoris*, overproduced, purified, and checked for activity with the use of proteoliposome vesicle shrinkage assays [supporting information (SI) Fig. S1*A*]. Rate constants of 14.1 s^{-1} and 21.3 s^{-1} were recovered with lipid-to-protein ratios of 130 and 65, respectively, demonstrating higher water transport activity than control vesicles lacking AQP5 (9.1 s^{-1}). In addition, purified AQP5 could be reversibly inhibited by $HgCl_2$ with an IC_{50} of 30 μM (Fig. S1*B*).

Crystals of AQP5 grew as stacked two-dimensional membranes (Fig. S2). This crystal form lacked the fourfold symmetry typically associated with AQP crystals (8, 12), notable exceptions being one structure of AQPZ at 3.2-Å resolution (14) and the open conformation of SoPIP2;1 at 3.9-Å resolution (12). Crystals of AQP5

Author contributions: R.H., K.N., M.F., A.B., P.K., U.J., and R.N. designed research; R.H., K.N., M.F., A.B., and S.T.-H. performed research; A.C.T.v.S. and J.K. contributed new reagents/analytic tools; R.H., K.N., P.K., U.J., and R.N. analyzed data; R.H., K.N., P.K., U.J., and R.N. wrote the paper.

The authors declare no conflict of interest.

This article is a PNAS Direct Submission.

Data deposition: The atomic coordinates and structure factor data have been deposited in the Protein Data Bank, www.pdb.org (PDB ID code 3D9S).

†R.H. and K.N. contributed equally to this work.

**To whom correspondence may be addressed. E-mail: urban.johanson@biochemistry.lu.se or richard.neutze@chem.gu.se.

This article contains supporting information online at www.pnas.org/cgi/content/full/0801466105/DCSupplemental.

Table 1. Crystallographic data and refinement statistics

Data collection	
Beamline/wavelength	ESRF ID14–3/0.931 Å
Resolution*, Å	52.6 − 2.0 (2.11 − 2.0)
Total observations/unique reflections*	311,242 (44,752)/84,751 (12,232)
Completeness*, %	82.9 (82.6)
Redundancy*	3.7 (3.7)
I/σ*	8.3 (1.5)
R_{sym}*†‡, %	6.1 (49.4)
Refinement	
Resolution, Å	10.0 − 2.0
R-factor§/R_{free}¶, %	16.2/19.3
Average B values, Å^2	37.2
RMS deviations from restraint target values	
Bond length/angle distances, Å	0.006/0.024
Ramachandran plot analysis (excluding glycine and proline)	
Most favored, %	83.8
Additional allowed, %	13.5
Generously allowed, %	1.5
Disallowed, %	1.2

*Values in parentheses are for the highest-resolution shell.
†$R_{sym} = \Sigma_h\Sigma_i|I_i(h)-\langle I(h)\rangle| / \Sigma_h\Sigma_i I(h)$, where $I_i(h)$ is the ith measurement.
‡The R_{sym} value for the last shell is high due to anisotropy. However, data are included because R-factor and R_{free} for the shell are low, which indicates that the data in this shell are still useful.
§R-factor $= \Sigma_h||F(h)_{obs}|-|F(h)_{calc}||/\Sigma_h|F(h)_{obs}|$.
¶R_{free} was calculated for 5% of reflections randomly selected in thin resolution shells (see *SI Text*).

diffracted to 2.0-Å resolution (Table 1) but suffered from nearly perfect pseudomerohedral twinning (30). The structure was solved by molecular replacement with the use of a homology model (*SI Text*) derived from the bovine AQP1 structure (8). Iterative rounds of model building with the use of special composite omit electron density maps compatible with twinning (*SI Text* and Fig. S3) and structural refinement converged to an R-factor of 16.2%, R_{free} of 19.3%, and twin ratio of 46.3%.

Crystal Structure of AQP5. Fig. 1*A* shows the refined structural model of the AQP5 tetramer, Fig. 1*B* overlays all four protomers, and Fig. 1*C* illustrates the $2F_{obs}-F_{calc}$ 2.0-Å electron density map for the water channel of protomer A. Between five and seven water molecules are unambiguously observed along the water transport channel in each of the protomers, six of which sit at conserved positions (Fig. 1*D*). All four protomers show similar water channel profiles when calculated by using HOLE (31) (Fig. S4), narrowing to an average radius of 1.02 Å near the highly conserved ar/R constriction region (7), which is marginally narrower than that of AQP1 (8) (1.18 Å, Fig. S4). In contrast with the 3.2-Å structure of AQPZ (14), Arg-188 of the ar/R constriction region has its side chain oriented toward the extracellular medium in all four protomers. Although minor variations in side-chain conformations are observed between protomers, the most significant structural difference is visible for the short C-terminal α-helix. In particular, a rocking movement over the full length of this helix is apparent when comparing the structures of protomers A and B (Movie S1).

Discussion

Conserved Triad. Comparison with other eukaryotic AQP structures (Table S1) shows that the N and C termini of AQP5 have a similar conformation to those of AQP0 (5, 6) and AQP1 (8) (Fig. S5*A*), in contrast with the conformation observed in SoPIP2;1 (Fig. S5*B*). Although loop D, which governs the gating of SoPIP2;1, adopts an open conformation in AQP5, the structure of the highly conserved Glu-4, Ser-83, Arg-86 triad (19) of AQP5 mimics the corresponding triad of SoPIP2;1 (12) (Glu-31, Ser-115, Arg-118; Fig. 2*A* and *B*), an arrangement that is unique for the mammalian AQP structures reported so far (4–8). In SoPIP2;1, this region has water-mediated hydrogen bond interactions that anchor loop D to loop B and maintain the plant AQP in its closed conformation (Fig. 2*B*) (12). Water-mediated and direct hydrogen bond interactions are also seen for the corresponding residues in AQP5, but in this case these interactions are with Ile-239 and Gly-241 of the C-terminal α-helix (Fig. 2*B*) anchoring this helix to loop B. Interestingly, AQP4, which lacks the conserved Glu of the triad, has been suggested to be gated by phosphorylation of Ser-111 (26), which corresponds to Ser-83 of AQP5. Phosphorylated Ser-111 in AQP4 could substitute for the Glu, allowing a similar interaction between loop B and the C terminus as observed for AQP5 (Fig. S5).

A Lipid Occludes the AQP5 Central Pore. Since the first AQP structures were obtained (7, 15), a potential transport role for the putative central pore (Fig. 1*A*, ○) along the pseudosymmetry axis of the AQP tetramer has been debated. Both experimental and theoretical studies have suggested the permeation of ions (32–34) and gas molecules (35–37) through the central pore of plant and mammalian AQPs. These ideas, however, are controversial because there is no apparent physiological role for AQP-mediated ion or gas transport in mammals (38), and CO_2 has high permeability through the lipid bilayer (39).

Because AQP5 crystallized in a space group lacking fourfold symmetry (Fig. S2), the axis along the center of the AQP tetramer does not coincide with a fourfold crystallographic axis; hence, the electron density does not become distorted by the effects of crystallographic symmetry. Fig. 3*A* shows the $2F_{obs}-F_{calc}$ composite omit electron density map along the central pore. Significant and continuous electron density which stretches two thirds of the way through the membrane is clearly visible, and structural features suggest a lipid head group near the cytosolic surface. Phosphatidylserine, which is present in both human and *P. pastoris* membranes (40), provides an optimal fit to this excess electron density.

Fig. 3*C* shows the final lipid model and refined $2F_{obs}-F_{calc}$ and $F_{obs}-F_{calc}$ electron density maps. The lipid head group is orientated by a network of hydrogen bonds to the backbone oxygen atoms of Arg-154 and Thr-155. The second chain of the lipid rests on the base of loop D (Gly-159 and Val-158 of the A and C protomers, respectively) and is disordered near its terminus. These interactions disrupt the perfect symmetry of the AQP tetramer and explain why AQP5 crystallized in a space group lacking fourfold symmetry. Calculation of the profile of the central pore shows that AQP5 contains a cavity that is significantly constricted near the extracellular surface (Fig. 3*B*, red zone). The lipid perfectly fills this cavity and occludes the central pore.

The situation is similar for the 3.2-Å structure of EcAQPZ (Fig. 3*D*, orange), for which a carbon chain of 14 atoms was built (14) from the periplasmic side of the membrane. In contrast, the profiles of the central pores of AQP0 (5, 6) and AQP1 (8), neither of which has been reported to contain lipids, show several highly constricted regions (Fig. 3*D*). In particular, Leu-167 of AQP5, which lies near the center of the membrane, corresponds to Phe-166 and Phe-176 in AQP0 and AQP1, respectively, and these bulky residues would prevent lipid insertion. Another constriction site in AQP0 and AQP1 lies near the cytosolic entrance to the central pore (Fig. 3*D*) and is created by a highly conserved glycine of loop D (Fig. S6*A*). In AQP5, this loop is anchored to helix 2 of the neighboring protomer via an extended hydrogen bond network (Fig. S7), and loop D adopts a slightly different conformation when compared with other mammalian AQPs, which helps to accommodate the lipid. It seems unlikely that this lipid plays an essential structural role in stabilizing the AQP5 tetramer because most AQPs have been crystallized in the

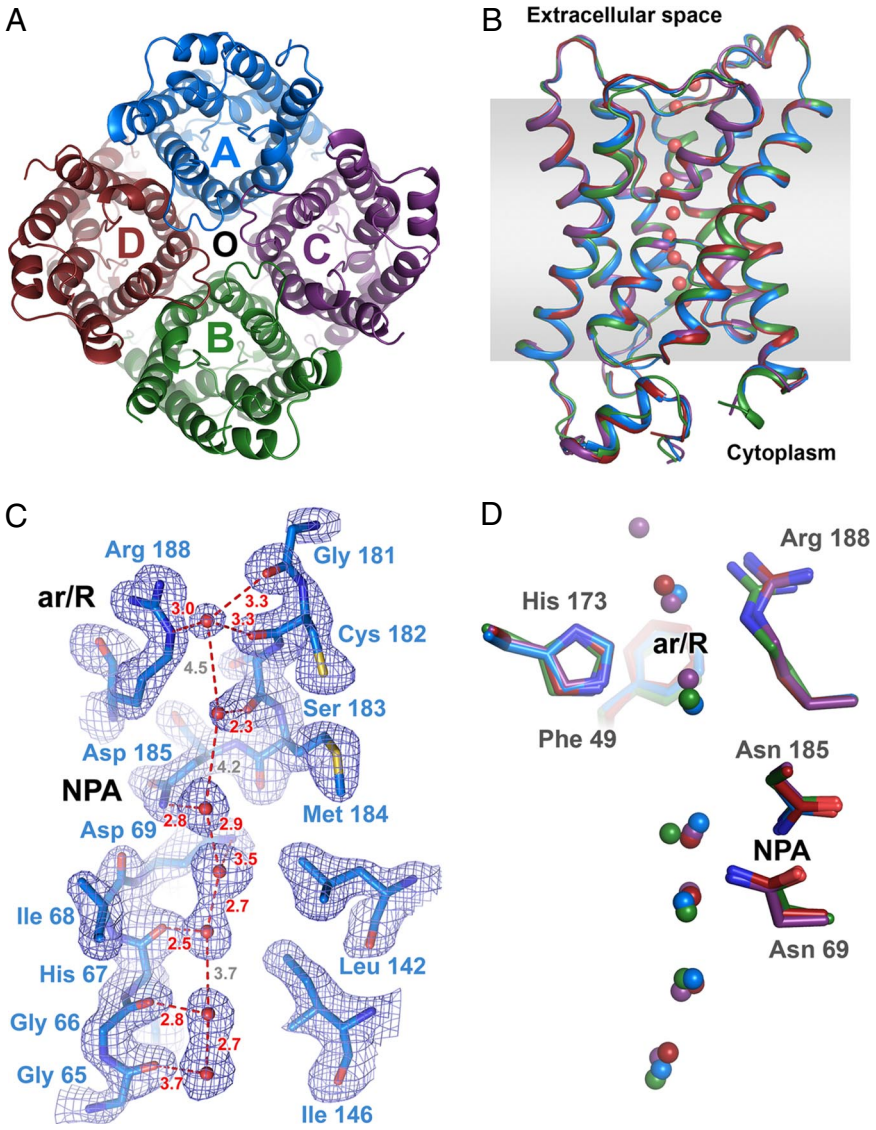

Fig. 1. Overview of human aquaporin 5. (*A*) Top view of the tetramer from the cytoplasm along the membrane normal. The protomers, *A-D*, are shown in blue, green, purple, and red, respectively. The water channel in each protomer is labeled (*A–D*). The putative central pore on the pseudofourfold axis of the tetramer is marked with ○. (*B*) Side view of a structural overlay of all four protomers parallel to the membrane, with the same color scheme as in *A*. Waters for protomer A and the approximate membrane are shown (red spheres and gray shading). (*C*) Example of the final $2F_{obs}-F_{calc}$ electron density maps (blue mesh contoured at 1.2 σ) for the water channel of protomer A (blue sticks). Waters (red spheres) and distances (red dashes) are shown. Positions of the conserved NPA motif and constriction region (ar/R) are shown. (*D*) Comparison of water positions in each channel of the four protomers, showing six conserved locations. Asparagine side chains in the NPA motifs and residues of the constriction region (ar/R) are shown. Waters and side chains are colored according to their protomer, as in *A*.

absence of a lipid within the central pore. Rather, a possible functional role for the lipid seems to be to occlude the pore and thereby prevent the transport of gas molecules or ions. These findings are consistent with the observations that deletion of AQP5 in rats leads to significantly reduced water permeability but does not affect CO_2 transport in the lung (38).

Trafficking of AQP5. It is established that chemical stimulation can induce the translocation of AQP5 from intracellular storage sites to the apical membrane (22–24). This is also true for AQP2, its closest paralog, which migrates to the plasma membrane on vasopressin stimulation, enhancing water resorption (2). A key event that signals AQP2 trafficking is the phosphorylation of a C-terminal site, Ser-256, by protein kinase A (41). Green fluorescent protein fusion studies have also implied that interference with the C terminus disturbs the trafficking patterns of both AQP2 (42) and AQP5 (24).

HsAQP5 contains several consensus phosphorylation sites (Fig. S6*B*); Ser-152 and Ser-156 (27, 43) in loop D and Thr-259 (24) in the C terminus have been discussed elsewhere, although no site has been unambiguously identified as essential for trafficking. Electron density for HsAQP5 extended as far as Pro-245; although this was further than any previous mammalian AQP structure, it did not allow the Thr-259 and Thr-263 phosphorylation sites to be observed. Thr-259 has been of particular interest because it is analogous to Ser-256 of AQP2 (41). However, the T259A mutation displayed a trafficking phenotype indistinguishable from that of wild-type AQP5 (24), and the Thr-263 site is not conserved in rat, mouse, or sheep, implying that these sites might not be essential for trafficking. Two other consensus phosphorylation sites, Ser-231 and Ser-233, are found near the C terminus of AQP5. The site at Ser-233 is conserved among human and plant AQPs and is equivalent to the site at Ser-274 of SoPIP2;1 (Fig. S6*B*), which is known to be phosphorylated in association with the gating of SoPIP2;1 (44). Ser-231 and Ser-233 are both located near the beginning of a short conserved C-terminal α-helix (residues 233 to 241, Fig. 2*A* and Fig. S6*B*) and face toward the cytoplasm, ensuring that they are accessible for phosphorylation. Comparison with structures of mammalian AQP0 and AQP1 (Fig. S5*A*), and between the protomers of AQP5 (Movie S1), suggests that this region is flexible and that phosphorylation at these positions may affect the local conformation. Alternatively, covalent modification of either of these residues may be directly recognized by other proteins without the need for conformational changes, resulting in trafficking.

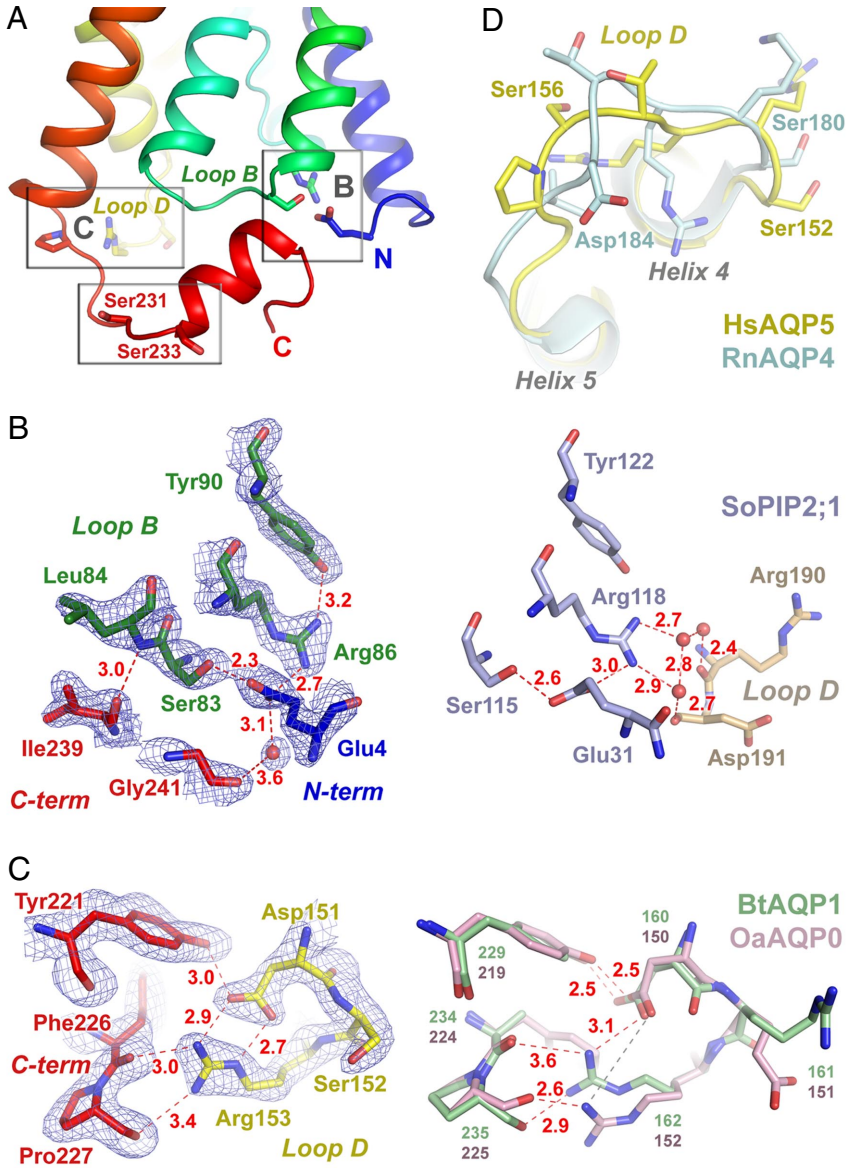

Fig. 2. Structural comparison of the conserved sites identified in AQP5. (*A*) Overview of the cytoplasmic half of AQP5 in cartoon representation with residues colored according to sequence numbering where the N and C termini are blue and red, respectively. Residues distant in sequence, highlighted by color difference, form key interactions (boxes B and C), shown in detail in *B* and *C*. A putative phosphorylation site in the C terminus is also boxed and the side chains of Ser-231 and Ser-233 are shown. (*B Left*) Zoom window for box B in *A* showing backbone and side chain interactions responsible for anchoring the N (blue) and C termini (red) to helix 3 (green) with $2F_{obs}-F_{calc}$ density map (blue mesh contoured at 1.2 σ). (*B Right*) Same view for SoPIP2;1 highlighting how conserved residues anchor loop D. (*C Left*) Zoom window for box C in *A* showing backbone and side-chain interactions responsible for anchoring the C terminus (red) to loop D (yellow) with $2F_{obs}-F_{calc}$ density map (blue mesh contoured at 1.2 σ). (*C Right*) Same view for AQP1 and AQP0 highlighting conserved residues. (*D*) Comparison of the conformation of loop D in AQP5 (yellow) and AQP4 (blue).

Two remaining consensus phosphorylation sites, Ser-152 and Ser-156 (27) of loop D, lie near the cytoplasmic surface (Fig. 2 *A* and *D*) and form a close association with the C terminus (Fig. 2*C*). Moreover, Ser-156 of AQP5 is phosphorylated by protein kinase A (43) and seems to be preferentially phosphorylated in tumors (45). As shown in Fig. 2*C*, the side chain of Arg-153 forms hydrogen-bond interactions with the backbone oxygen atoms of Phe-226 and Pro-227, and these interactions are well conserved compared with other mammalian AQP structures (4, 8) (Fig. 2*C*). It seems therefore that the phosphorylation of either Ser-152 or Ser-156 could induce significant conformational changes within loop D, potentially disrupting the hydrogen-bond interactions between Arg-153, Phe-226, and Pro-227 that anchor the C-terminal α-helix of AQP5 to loop D. In this regard, it is noteworthy that Ser-156 corresponds to an aspartate residue in AQP4, for which the conformation of loop D is significantly displaced relative to that of AQP5 (Fig. 2*D*) and the C-terminal α-helix is not visible (10). Although it is unclear whether the conformation of loop D in AQP4 mimics that of AQP5 with Ser-156 phosphorylated, different conformational states of the C-terminal α-helix of AQP5 are apparent when comparing the structures of protomers A and B (Movie S1), indicating flexibility. Thus conformational changes within this region may be a mechanism through which the protein flags trafficking.

Work remains to unambiguously identify the posttranslational modifications that signal trafficking events and gating in human AQPs *in vivo*. Nevertheless, the high-resolution x-ray structure of human AQP5 provides essential clues suggesting how AQP5 might signal trafficking and will guide further biochemical and physiological investigation. As a more complete structural picture of the key ingredients signaling AQP5 trafficking emerges, it will have broad implications concerning the underlying mechanism of membrane protein trafficking in human cells.

Materials and Methods

For details see *SI Text*.

Cloning, Overproduction, and Membrane Preparation. The cDNA encoding HsAQP5 was subcloned into pPICZB (Invitrogen) from IMAGE clone ID 5269384

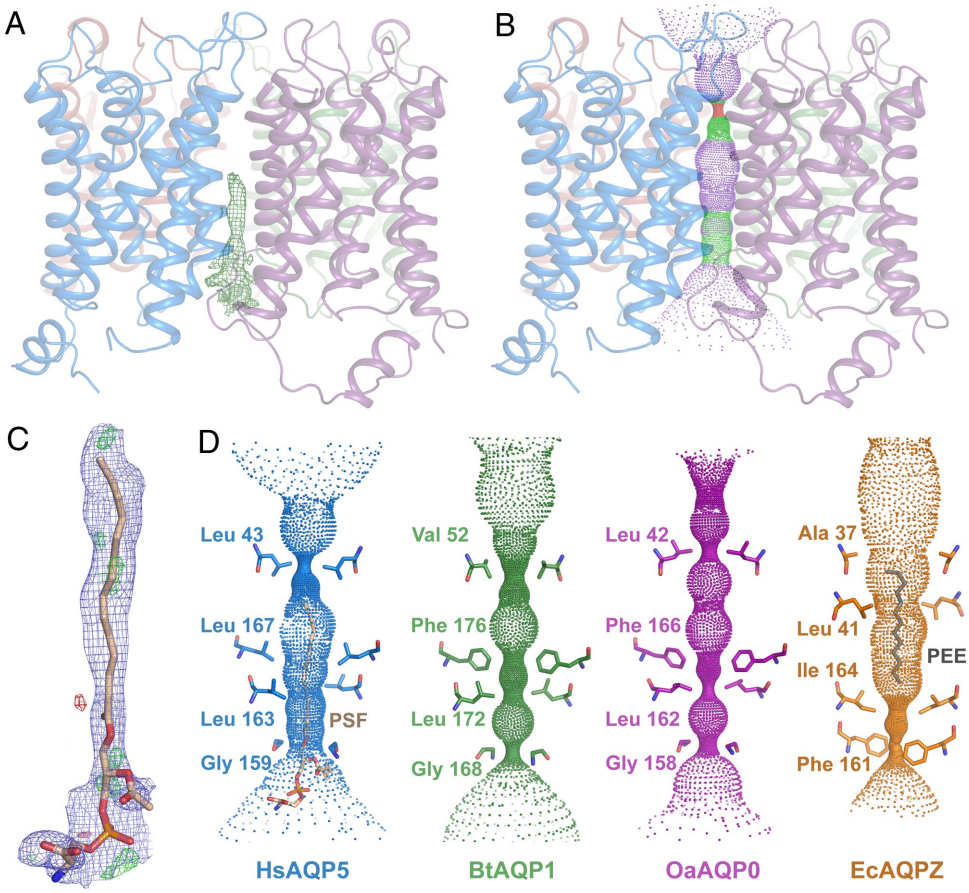

Fig. 3. Lipid blocking the putative central pore of the AQP5 tetramer. (*A*) Overview of the tetramer, viewed parallel to the membrane, showing continuous excess electron density in the composite omit map (green mesh contoured at 1.2 σ), at the center of the tetramer. (*B*) Identical to *A* but showing the profile of the central pore calculated by HOLE. Red and green zones identify constricted and open regions, respectively. (*C*) Final refined model for the lipid with $2F_{obs}-F_{calc}$ map (blue mesh contoured at 0.9 σ). Positive (light green) and negative (red) peaks in the $F_{obs}-F_{calc}$ map are also shown (contoured at 2.8 and -2.8 σ, respectively). (*D*) HOLE representation of the profile of the central pores of HsAQP5 (blue) compared with BtAQP1 (green), OaAQP0 (purple), and EcAQPZ (orange). Side chains constricting the pores are shown for two opposite protomers in each case. Lipid molecules found in the central pores of AQP5 (phosphatidylserine, PSF) and AQPZ (phosphatidylethanolamine, PEE) are also shown in beige and gray, respectively.

via PCR. The construct was cloned into *P. pastoris* (X-33) according to EasySelect Pichia Expression Kit (Invitrogen). The transformant with the highest expression level was selected by Western blotting with the use of antibodies directed against the C terminus of rat AQP5 (Alpha Diagnostic). Cultures were grown in baffled flasks for 75 h with addition of methanol every 24 h. Cells where harvested by centrifugation and broken with the use of a Bead Beater, and membranes were pelleted.

Solubilization, Purification and Crystallization. Membranes containing ~30 mg of protein were diluted with buffer containing 6% n-nonyl-β-D-glucopyranoside (Anatrace) and stirred at room temperature for 1 h. All subsequent purification steps were performed at 8°C according to *SI Text*. Crystals were grown by hanging drop vapor diffusion at 8°C by mixing protein and reservoir solution in a 1:1 ratio. Initial crystals of AQP5 grew in 0.1 M Tris·HCl, pH 7.0, 0.1 M NaCl, and PEG 400. Additive screening yielded a final optimal condition of 0.1 M Tris·HCl, pH 7.6, 0.1 M NaCl, 19% PEG 400, 6% (vol/vol) 1,6-hexanediol and 3% (vol/vol) 1,4-butanediol or 3% (vol/vol) 1,3-propanediol. Crystals appeared within 5–10 days and reached a maximum size of $0.2 \times 0.2 \times 0.1$ mm. Crystals were flash-frozen in liquid nitrogen.

Data Collection and Structure Determination. Diffraction data were collected at 100 K at ESRF, France. Crystals diffracted to 1.8-Å resolution, belonged to the orthorhombic space group $P2_12_12_1$ (a = 90.48 Å, b = 90.64 Å, c = 184.39 Å), contained one tetramer per asymmetric unit, and were nearly perfectly pseudomerohedrally twinned; see *SI Text* for details. Data were processed and scaled with Mosflm (46) and Scala (47). The structure was solved by molecular replacement (*SI Text*). The entire structure was checked and manually rebuilt into $2F_{obs}-F_{calc}$, $F_{obs}-F_{calc}$, and special composite omit maps suitable for twinned data by using Coot (48) in several iterative rounds. Computational refinement was made in SHELX (49) to account for the twin operator and twin fraction. The AQ5 model contains four protomers, A through D, with amino acids 1–245, 1–245, 3–245, and 1–245, respectively, 117 water molecules, and a phosphatidylserine lipid molecule.

ACKNOWLEDGMENTS. We thank Remco Wouts for rewriting the omit map script in Perl and Anders Bay Pederson for producing Movie S1. This work was supported by VR, E-MEP, Carl Tryggers Stiftelse, Stiftelsen Olle Engkvist Byggmästare, University of Gothenburg Quantative Biology Platform, Formas, and the Research School in Pharmaceutical Sciences (FLÄK).

1. Preston GM, Carroll TP, Guggino WB, Agre P (1992) Appearance of water channels in Xenopus oocytes expressing red cell CHIP28 protein. *Science* 256:385–387.
2. King LS, Kozono D, Agre P (2004) From structure to disease: The evolving tale of aquaporin biology. *Nat Rev Mol Cell Biol* 5:687–698.
3. Krane CM, Goldstein DL (2007) Comparative functional analysis of aquaporins/glyceroporins in mammals and anurans. *Mamm Genome* 18:452–462.
4. Gonen T, Sliz P, Kistler J, Cheng Y, Walz T (2004) Aquaporin-0 membrane junctions reveal the structure of a closed water pore. *Nature* 429:193–197.
5. Harries WE, Akhavan D, Miercke LJ, Khademi S, Stroud RM (2004) The channel architecture of aquaporin 0 at a 2.2 Å resolution. *Proc Natl Acad Sci USA* 101:14045–14050.
6. Gonen T, *et al.* (2005) Lipid-protein interactions in double-layered two-dimensional AQP0 crystals. *Nature* 438:633–638.
7. Murata K, *et al.* (2000) Structural determinants of water permeation through aquaporin-1. *Nature* 407:599–605.
8. Sui H, Han BG, Lee JK, Walian P, Jap BK (2001) Structural basis of water-specific transport through the AQP1 water channel. *Nature* 414:872–878.

9. Schenk AD, *et al.* (2005) The 4.5 A structure of human AQP2. *J Mol Biol* 350:278–289.
10. Hiroaki Y, *et al.* (2006) Implications of the aquaporin-4 structure on array formation and cell adhesion. *J Mol Biol* 355:628–639.
11. Kukulski W, *et al.* (2005) The 5 Å structure of heterologously expressed plant aquaporin SoPIP2;1. *J Mol Biol* 350:611–616.
12. Törnroth-Horsefield S, *et al.* (2006) Structural mechanism of plant aquaporin gating. *Nature* 439:688–694.
13. Savage DF, Egea PF, Robles-Colmenares Y, O'Connell JD, Stroud RM (2003) Architecture and selectivity in aquaporins: 2.5 Å X-ray structure of aquaporin Z. *PLoS Biol* 1:E72.
14. Jiang J, Daniels BV, Fu D (2006) Crystal structure of AqpZ tetramer reveals two distinct Arg-189 conformations associated with water permeation through the narrowest constriction of the water-conducting channel. *J Biol Chem* 281:454–460.
15. Fu D, *et al.* (2000) Structure of a glycerol-conducting channel and the basis for its selectivity. *Science* 290:481–486.
16. Lee JK, Kozono D, Remis J, Kitagawa Y, Agre P, Stroud RM (2005) Structural basis for conductance by the archaeal aquaporin AqpM at 1.68 A. *Proc Natl Acad Sci USA* 102:18932–18937.
17. Wang Y, Tajkhorshid E (2007) Molecular mechanisms of conduction and selectivity in aquaporin water channels. *J Nutr* 137:1509S–1515S.
18. de Groot BL, Grubmüller H (2005) The dynamics and energetics of water permeation and proton exclusion in aquaporins. *Curr Opin Struct Biol* 15:176–183.
19. Hedfalk K, *et al*. (2006) Aquaporin gating. *Curr Opin Struct Biol* 16:447–456.
20. Han Z, Patil RV (2000) Protein kinase A-dependent phosphorylation of aquaporin-1. *Biochem Biophys Res Commun* 273:328–332.
21. de Mattia F, *et al.* (2005) Lack of arginine vasopressin-induced phosphorylation of aquaporin-2 mutant AQP2–R254L explains dominant nephrogenic diabetes insipidus. *J Am Soc Nephrol* 16:2872–2880.
22. Yang F, Kawedia JD, Menon AG (2003) Cyclic AMP regulates aquaporin 5 expression at both transcriptional and post-transcriptional levels through a protein kinase A pathway. *J Biol Chem* 278:32173–32180.
23. Ishikawa Y, *et al.* (2005) Identification of AQP5 in lipid rafts and its translocation to apical membranes by activation of M3 mAChRs in interlobular ducts of rat parotid gland. *Am J Physiol Cell Physiol* 289:C1303–C1311.
24. Kosugi-Tanaka C, Li X, Yao C, Akamatsu T, Kanamori N, Hosoi K (2006) Protein kinase A-regulated membrane trafficking of a green fluorescent protein-aquaporin 5 chimera in MDCK cells. *Biochim Biophys Acta* 1763:337–344.
25. Garcia F, *et al.* (2001) The water channel aquaporin-8 is mainly intracellular in rat hepatocytes, and its plasma membrane insertion is stimulated by cyclic AMP. *J Biol Chem* 276:12147–12152.
26. Gunnarson E, *et al*. (2008) Identification of a molecular target for glutamate regulation of astrocyte water permeability. *Glia* 56:587–596.
27. Raina S, Preston GM, Guggino WB, Agre P (1995) Molecular cloning and characterization of an aquaporin cDNA from salivary, lacrimal, and respiratory tissues. *J Biol Chem* 270:1908–1912.
28. Wellner RB, Hong S, Cotrim AP, Swaim WD, Baum BJ (2005) Modifying the NH2 and COOH termini of aquaporin-5: Effects on localization in polarized epithelial cells. *Tissue Eng* 11:1449–1458.
29. Tsubota K, Hirai S, King LS, Agre P, Ishida N (2001) Defective cellular trafficking of lacrimal gland aquaporin-5 in Sjogren's syndrome. *Lancet* 357:688–689.
30. Terwisscha van Scheltinga AC, Valegard K, Hajdu J, Andersson I (2003) MIR phasing using merohedrally twinned crystals. *Acta Crystallogr D Biol Crystallogr* 59:2017–2022.
31. Smart OS, Goodfellow JM, Wallace BA (1993) The pore dimensions of gramicidin A. *Biophys J* 65:2455–2460.
32. Yool AJ, Stamer WD, Regan JW (1996) Forskolin stimulation of water and cation permeability in aquaporin 1 water channels. *Science* 273:1216–1218.
33. Anthony TL, *et al*. (2000) Cloned human aquaporin-1 is a cyclic GMP-gated ion channel. *Mol Pharmacol* 57:576–588.
34. Yu J, Yool AJ, Schulten K, Tajkhorshid E (2006) Mechanism of gating and ion conductivity of a possible tetrameric pore in aquaporin-1. *Structure* 14:1411–1423.
35. Prasad GV, Coury LA, Finn F, Zeidel ML (1998) Reconstituted aquaporin 1 water channels transport CO2 across membranes. *J Biol Chem* 273:33123–33126.
36. Wang Y, Cohen J, Boron WF, Schulten K, Tajkhorshid E (2007) Exploring gas permeability of cellular membranes and membrane channels with molecular dynamics. *J Struct Biol* 157:534–544.
37. Uehlein N, Lovisolo C, Siefritz F, Kaldenhoff R (2003) The tobacco aquaporin NtAQP1 is a membrane CO_2 pore with physiological functions. *Nature* 425:734–737.
38. Fang X, Yang B, Matthay MA, Verkman AS (2002) Evidence against aquaporin-1-dependent CO2 permeability in lung and kidney. *J Physiol* 542:63–69.
39. Hub JS, de Groot BL (2006) Does CO_2 permeate through aquaporin-1? *Biophys J* 91:842–848.
40. Opekarova M, Tanner W (2003) Specific lipid requirements of membrane proteins–a putative bottleneck in heterologous expression. *Biochim Biophys Acta* 1610:11–22.
41. Fushimi K, Sasaki S, Marumo F (1997) Phosphorylation of serine 256 is required for cAMP-dependent regulatory exocytosis of the aquaporin-2 water channel. *J Biol Chem* 272:14800–14804.
42. Gustafson CE, *et al.* (1998) Vasopressin regulated trafficking of a green fluorescent protein-aquaporin 2 chimera in LLC-PK1 cells. *Histochem Cell Biol* 110:377–386.
43. Woo J, *et al.* (2008) Membrane trafficking of AQP5 and cAMP dependent phosphorylation in bronchial epithelium. *Biochem Biophys Res Commun* 366:321–327.
44. Johansson I, Larsson C, Ek B, Kjellbom P (1996) The major integral proteins of spinach leaf plasma membranes are putative aquaporins and are phosphorylated in response to Ca^{2+} and apoplastic water potential. *Plant Cell* 8:1181–1191.
45. Woo J, *et al.* (2008) Overexpression of AQP5, a putative oncogene, promotes cell growth and transformation. *Cancer Lett* 264:54–62.
46. Leslie AGW (1992) Recent changes to the MOSFLM package for processing film and image plate data. *Joint CCP4 and ESF-EAMCB Newsletter on Protein Crystallography* 26.
47. Kabsch W (1993) Automatic processing of rotation diffraction data from crystals of initially unknown symmetry and cell constants. *J Appl Cryst* 26:785–800.
48. Emsley P, Cowtan K (2004) Coot: Model-building tools for molecular graphics. *Acta Crystallogr D Biol Crystallogr* 60:2126–2132.
49. Sheldrick GM (2008) A short history of SHELX. *Acta Crystallogr A* 64:112–122.